Insight into the role of the Bateman domain at the molecular and physiological levels through engineered IMPDHs

Antoine Gedeon, Nour Ayoub, Sébastien Brûlé, Bertrand Raynal, Gouzel Karimova, Muriel Gelin, Ariel Mechaly, Ahmed Haouz, Gilles Labesse, Hélène Munier-Lehmann

Insight into the role of the Bateman domain at the molecular and physiological levels through engineered IMPDHs

Antoine Gedeon[1#], Nour Ayoub[1‡], Sébastien Brûlé[2], Bertrand Raynal[2], Gouzel Karimova[3], Muriel Gelin[4], Ariel Mechaly[5], Ahmed Haouz[5], Gilles Labesse[4], Hélène Munier-Lehmann[1‡*]

[1]Institut Pasteur, Université Paris Cité, CNRS UMR3523, Unité de Chimie et Biocatalyse, F-75015 Paris, France.

[2]Institut Pasteur, Université Paris Cité, Plate-Forme de Biophysique Moléculaire, C2RT, CNRS UMR3528, F-75015 Paris, France

[3]Institut Pasteur, Université Paris Cité, Unité de Biochimie des Interactions Macromoléculaires, CNRS UMR3528, F-75015 Paris, France

[4]Centre de Biologie Structurale, Université Montpellier, INSERM, CNRS, F-34090 Montpellier, France

[5]Institut Pasteur, Université Paris Cité, Plate-Forme de Cristallographie, C2RT, CNRS UMR3528, F-75015 Paris, France

Present address : Institut Pasteur, Université Paris Cité, CNRS UMR3525, Unité de Microbiologie Structurale, F-75015 Paris, France.

‡ Present address : Institut Pasteur, Université Paris Cité, CNRS UMR3523, Plate-Forme de Criblage Chémogénomique et Biologique, F-75015 Paris, France.

*To whom correspondence should be addressed

e-mail: helene.munier-lehmann@pasteur.fr

This article has been accepted for publication and undergone full peer review but has not been through the copyediting, typesetting, pagination and proofreading process which may lead to differences between this version and the Version of Record. Please cite this article as doi: 10.1002/pro.4703
Received: Mar 03, 2023;Revised: May 15, 2023;Accepted: Jun 06, 2023

Abstract

Inosine 5'-monophosphate dehydrogenase (IMPDH) is a^ ubiquitous enzyme that catalyzes the NAD^+-dependent oxidation of inosine 5'-monophosphate into xanthosine 5'-monophosphate. This enzyme is formed of two distinct domains, a core domain where the catalytic reaction occurs, and a less-conserved Bateman domain. Our previous studies gave rise to the classification of bacterial IMPDHs into two classes, according to their oligomeric and kinetic properties. MgATP is a common effector but leading to different effects when it binds within the Bateman domain: it is either an allosteric activator for class I IMPDHs or a modulator of the oligomeric state for class II IMPDHs.To get insight into the role of the Bateman domain in the dissimilar properties of the two classes, deleted variants of the Bateman domain and chimeras issued from the interchange of the Bateman domain between the three selected IMPDHs have been generated and characterized using an integrative structural biology approach. Biochemical, biophysical, structural and physiological studies of these variants unveil the Bateman domain as being the carrier of the molecular behaviors of both classes.

Introduction

Multiple levels of enzyme activity regulation are indispensable to maintain delicate homeostatic concentrations of metabolites in cells. On a genetic level, enzyme expression can be controlled by selective induction or repression of gene expression or by other higher-order regulations during the translation of mRNA[1]. On a protein level, covalent regulations by post-translational modifications or shorter-term regulations *via* the binding of effectors can occur. One of the most intriguing forms of this latter mode is allosteric regulation of multidomain proteins (representing around 65% and 80% of prokaryotes and eukaryotes proteomes, respectively[2]). Allostery is defined as a correspondence of conformational changes after the binding of a regulatory agent at a distal site from the active site that consequently activates or inhibits enzyme activity. This molecular behavior has been studied for many decades, and several kinetic/thermodynamic models have been proposed, the most famous being the concerted Monod-Wyman-Changeux model[3-5] and the sequential Koshland-Némethy-Filmer (or induced fit) model[6]. At the structural level, various mechanisms can be involved in allosteric regulation and are still debated or to be unraveled. An example of such a regulatory domain is the so-called Bateman domain (BD) that was first identified in 1997[7]. This domain is a small regulatory domain composed of a pair of interleaved ßαßßα motifs in cystathionine β-synthase (and therefore named CBS motifs). Since then, several proteins were identified as containing Bateman domains in all living organisms, one of which is inosine 5'-monophosphate dehydrogenase (IMPDH)[8,9]. The role of CBS motifs in nucleo(s/t)ide binding was recognized much later and demonstrated for IMPDH in 2013[10].

IMPDH (E.C. 1.1.1.205) plays a crucial role in nucleotide metabolism by catalyzing the first committed step in *de novo* guanine nucleotide biosynthesis (Fig. 1a). The enzymatic reaction

carried out by IMPDH is a nicotinamide adenine dinucleotide (NAD^+)-dependent oxidation on the carbon 2 of the purine cycle of inosine 5'-monophosphate (IMP) into xanthosine 5'-monophosphate (XMP) (Fig. 1b). The canonic topological form of IMPDHs is evolutionarily conserved and consists of two structural domains, a $(ß/α)_8$-barrel core catalytic domain, and a Bateman domain (Fig. 2 and Extended data Fig. 1a). Several point mutations within the Bateman domain were linked to diseases[11]. For example, in human IMPDH1, substitution mutations in the Bateman domain were associated with autosomal dominant retinitis pigmentosa and Leber congenital amaurosis[12-14].

In most CBS motifs[11,15,16], the presence of two ligand-binding sites has been demonstrated. Moreover, a preference for nucleo(s/t)idic compounds (such as ATP, S-methyl-5'-thioadenosine (MTA) or NAD^+) was observed. In our previous studies, we identified MgATP as an allosteric effector of IMPDHs following binding into two sites within the Bateman domain[10,17]. We recently proposed a classification of bacterial IMPDHs into two classes according to the regulation of their catalytic properties and quaternary structures[18]. Class I IMPDHs are described as activated by MgATP and are always octameric in solution in all tested conditions. An unprecedented positive homotropic cooperativity toward IMP but not NAD^+ was also noted, with a Hill number index slightly higher than 1. Three IMPDHs, all being from Gram-negative bacteria (*Pseudomonas aeruginosa*, *Legionella pneumophila* and *Neisseria meningitidis*), were described as members of the class I. Reciprocally, class II IMPDHs behave as Michaelis-Menten enzymes for both substrates (IMP and NAD^+), and no effect of MgATP on kinetic parameters was observed. Nonetheless, MgATP induces an oligomeric state shift: the apo form is a tetramer that switches to an octamer in the presence of saturating concentrations of MgATP or NAD^+. This class groups orthologs from both Gram-positive and Gram-negative bacteria (such as *Burkholderia thailandensis*, *Staphylococcus aureus* and *Klebsiella pneumoniae*). We also found that human IMPDH1 is a

member of this class II and is capable of forming fibers in the presence of MgATP[10]. Ultimately, the characterization of other IMPDHs from eukaryotic organisms reported by other groups also showed identical regulation by MgATP as of class II bacterial IMPDHs, *i.e.* for IMPDH of fungi *Ashbya gossypii*[19], and human IMPDH1 and IMPDH2 isoforms[20-22].

As neither sequence signatures nor obvious structural differences in the catalytic domain were clearly attributed to one or another class, we wonder if the definition of the mode of MgATP-regulation could be narrowed down to the Bateman domain. Therefore, in the present work, we investigated the protein domain-function relationship of the Bateman domain in the differential regulation of class I and class II IMPDHs. We report a multidisciplinary characterization of two types of IMPDH variants obtained either by deletion of the Bateman domain or by chimeragenesis based on the interchange of Bateman domains between representatives of both classes. Our results provide evidence that illustrates a *bona fide* role of the Bateman domain as a carrier of regulatory properties of quaternary structure and catalytic activity of IMPDHs. We further showed that the Bateman domain is also determinant of bacterial growth rates, illustrating a physiological role of this domain *in vivo*.

Results

All canonic monomeric forms of bacterial IMPDHs share a common architecture formed of a regulatory Bateman domain (BD) nested within a loop of a catalytic $(\beta/\alpha)_8$ barrel-domain (CD), which is therefore divided into two fragments, noted CD1 and CD2 (Fig. 2 and Extended data Fig. 1a). The IMPDHs of *E. coli* (noted IMPDHec), *P. aeruginosa* (noted IMPDHpa) and *B. thailandensis* (noted IMPDHbt) share a high sequence identity (Extended data Fig. 1b-d) but differ in their biochemical properties and homo-oligomeric structures. IMPDHpa[10] (class I IMPDH) is octameric in all tested conditions and the only one of the three to be activated by MgATP, whereas IMPDHbt[18] (class II IMPDH) is tetrameric and switches to an octamer in the presence of MgATP. In this work, we first characterized the biochemical and biophysical properties of IMPDHec as previously performed for the two other selected IMPDHs[10,18].

Allosteric regulation of IMPDHec by MgATP

IMPDHec was overexpressed in *E. coli* and purified in a two-step procedure (see Materials and Methods, and Extended data Fig. 2a). In size exclusion chromatography, IMPDHec eluted in multiple peaks, indicating that the enzyme seems to coexist under several oligomeric states (Extended data Fig. 3a). Measurement of IMP dehydrogenase activity showed no differences in specific activities of detected IMPDHec species. This observation is in agreement with previous analytical ultracentrifugation (AUC) studies on IMPDHec which showed the existence of several states in its apo form, with sedimentation coefficients ranging from 6.4 S (tetramer) to 17.8 S (octamer)[23]. Using static light scattering analysis (SEC-SLS), we were able to detect IMPDHec stabilization in an octameric form or a tetrameric form in the presence of MgATP or IMP, respectively (Extended data Fig. 3b).

We next studied the effect of MgATP on the catalytic activity of IMPDHec by monitoring the formation of NADH at 340 nm. Our results showed no effect of MgATP on kinetics (Tables 1 and 2, Extended data Fig. 3c-e), as previously described by other groups[24,25]. Thus, these data confirm that IMPDHec presents class II-like properties, with MgATP being a modulator of quaternary structure but not of the catalytic activity.

Design and expression of recombinant IMPDH variants

With the three parent enzymes IMPDHpa, IMPDHbt and IMPDHec chosen as scaffolds, we generated two types of IMPDH variants (Fig. 2). The first type of variants (noted ΔBD) consisted of IMPDH with a deleted Bateman domain. To construct them, the corresponding ORFs were generated by amplifying separately the CD1 and CD2 of interest with 5'-3' overlap extensions that are then reassembled by a primerless PCR. The second type of variants consisted of IMPDH chimera exhibiting exchange of catalytic and regulatory domains between IMPDHpa and IMPDHec or IMPDHbt to produce a protein with a class I catalytic domain and a class II Bateman domain and vice versa. The corresponding ORFs were generated using the same strategy as for the ΔBD (except for IMPDH CDpa BDbt, for which the construct was purchased from Twist Bioscience), but in this case between CD1, BD and CD2 of interest. For simplicity, we used the chimeric enzyme nomenclature as depicted in Fig. 2 and Extended data Table 1: for example, IMPDH CDpa BDec corresponds to the chimera harboring the catalytic domain of IMPDHpa and the Bateman domain of IMPDHec.

The different mutant ORFs were then cloned into pET28a and expressed in either of the three *E. coli* strains: BL21(DE3)/pDIA17[26], or BL21 Star™ (DE3) (Thermo Fisher Scientific) or BL21 (DE3)/pGro7 (Chaperone BL21(DE3), Takara). All recombinant proteins were

obtained in the soluble extract after sonication (see Materials and Methods, and Extended data Fig. 2a with IMPDHec ΔBD as an example).

The variants were purified in a two-step procedure (as for IMPDHec) at over 95% purity as indicated by SDS-PAGE (Extended data Fig. 2b). Samples were tested for integrity, purity and solubility according to published recommendations[27]. Thus, dynamic light scattering (DLS) experiments were performed to optimize purification and storage conditions (Extended data Table 1) in order to increase the homogeneity and the stability of the recombinant protein samples.

Steady-state kinetic properties of IMPDH variants

All purified proteins were active *in vitro* since an NAD^+-dependent dehydrogenase activity in the presence of the substrate IMP was detected. Similar to other characterized IMPDHs[8], all variants were also found to be K^+-dependent enzymes, thus specific kinetic buffers (buffer K, refer to Extended data Table 1) containing a minimal concentration of at least 25 mM of potassium chloride were selected.

To investigate the effect of MgATP on the catalytic activity of the different variants, we conducted enzymatic assays in the absence or in the presence of this effector, and at a saturating concentration of one substrate and variable concentrations of the other (Fig. 3 and Extended data Fig. 4 and 5). The curves correspond to the fit of the experimental data to the Michaelis-Menten or the substrate inhibition equations (see Materials and Methods) and the calculated kinetic parameters are displayed in Tables 1 and 2.

All ΔBD variants showed to be two to four-fold more active (Extended data Fig. 4a) and exhibited higher maximum velocities in comparison with the corresponding wild-type forms (Tables 1 and 2). This suggested that in all the wild-type IMPDHs the Bateman domains play an inhibitory role. Additionally, representative plots of dehydrogenase activity of IMPDHbt

ΔBD and IMPDHec ΔBD as a function of concentrations of IMP or NAD^+ were all hyperbolic (Fig. 3a-b and Extended data Fig. 5a-b), indicating Michaelis-Menten-type kinetics, except for IMPDHbt ΔBD, to which a slight inhibition by excess of NAD^+ was observed ($K_i^{NAD^+}$ = 7.5 ± 2.1 mM). For both variants, affinity constants for IMP were close to those of the corresponding wild-type forms (Table 1), whereas a lower affinity for the second substrate (NAD^+) was observed (Table 2). Not unexpectedly, as the binding sites of MgATP located in the Bateman domain have been deleted, no effect of MgATP on the catalytic activity of any ΔBD variants was observed (Extended data Fig. 4c-d, Tables 1 and 2).

On the other hand, all chimeras exhibited loss or gain of MgATP activation, depending on the class of the transplanted Bateman domain (Extended data Fig. 4e-h). In the case of IMPDH CDec BDpa and IMPDH CDbt BDpa, both containing a class II catalytic domain and a class I Bateman domain, all IMP (Fig. 3c-d) or NAD^+ (Extended data Fig. 5c-d)-dependency variations were hyperbolic, except for IMPDH CDbt BDpa, to which a slight inhibition by excess of NAD^+ in the absence of MgATP was noted. MgATP was shown to be, as in wild-type class I IMPDHs, an activator, that increases the affinity to IMP (Table 1). This effector also increased the maximum velocity for the chimera IMPDH CDbt BDpa (Fig. 3d, Extended data Fig 5d). For IMPDH CDpa BDec and IMPDH CDpa BDbt, composed of a class I catalytic core and a class II Bateman domain, MgATP did not exert positive heterotropic response (Extended data Fig. 4g-h, Fig. 3e-f and Extended data Fig. 5e-f). Moreover, these chimeras exhibited loss of the positive cooperativity towards IMP, a characteristic of wild-type IMPDHpa[10]. Thus, the four chimeras share similar kinetic properties as the IMPDH which the Bateman domain was derived from.

To summarize, all the data indicate that the Bateman domain of both IMPDH classes plays a key role in the auto-regulation of the dehydrogenase activity and is the carrier of the differential kinetic behaviors.

Oligomeric state regulation of IMPDH mutants

To check whether the Bateman domain is also essential and determinant for the quaternary structure organization, we analyzed the oligomeric state and hydrodynamic shape in solution of the generated variants. Therefore, we started by performing analytical ultracentrifugation (AUC) analysis and investigated the effect of saturating concentrations of different ligands (IMP, NAD^+ and MgATP). All sedimentation data are recapitulated in Table 3.

Concerning the ΔBD variants, we have previously shown that IMPDHpa ΔBD is insensitive to MgATP and coexists in an equilibrium between tetrameric and octameric forms[10]. In the case of IMPDHec ΔBD and IMPDHbt ΔBD, the observed MgATP- or NAD^+-induced oligomerization switch in the case of wild-type counterparts[18] was lost upon Bateman domain deletion. However, in the absence of any ligand, IMPDHec ΔBD is in a tetramer-octamer equilibrium ($S_{20,w}$ of 9.1S and 11.7S, respectively), and IMPDHbt ΔBD is solely tetrameric ($S_{20,w}$ = 7.9S) at 1 mg/mL.

The two chimeras IMPDH CDec BDpa (Fig. 4a) and CDbt BDpa (Extended data Fig. 6a) are octameric in all tested conditions with no trace of any tetrameric species. Frictional ratios ranged from 1.30 to 1.50, which are compatible with ellipsoidal shapes and mild conformational changes mediated by the different ligands. Indeed, the sedimentation distribution peak of MgATP-bound form of IMPDH CDec BDpa is shifted to higher sedimentation values in comparison with other conditions, proposing a slightly less elongated conformation in the presence of this allosteric effector (Fig 4a, blue curve). This is also accompanied with a decrease of frictional ratio in the presence of MgATP in comparison with the apo condition (Table 3), meaning that binding of the effector induces indeed a compaction of the octamer towards a more globular shape. On the other hand, the last two chimeras IMPDH CDpa BDec and CDpa BDbt exist either as a tetramer or an octamer, or

both in equilibrium, depending on the tested conditions (Table 3, Fig. 4d and Extended data Fig. 6c). For IMPDH CDpa BDec, in the absence of any ligand, two species are observed but in different proportions depending on the protein concentration: at 0.1 mg/mL (Extended data Fig. 6c), a predominant tetrameric population (64%) and octameric species (36%) are present with sedimentation coefficients of 8.9S and 13.1S, respectively, whereas at 2 mg/mL (Extended data Fig. 6d) an octameric population is predominant (87%) with the tetrameric species being in lower amount (13%). However, addition of IMP or MgATP shifted the oligomeric state of the enzyme into a tetramer ($S_{20,w}$ = 7.8S) or an octamer ($S_{20,w}$ = 14.5S) respectively, as expected for class II IMPDHs. Interestingly, the sedimentation coefficient increases as the frictional ratio decreases for this chimera in the presence of MgATP, which is yet again illustrative of MgATP-induced compaction. In the presence of NAD^+, again the octameric species are predominant (Fig 4d, green curve). Thus, even though the quaternary structure in the apo condition of IMPDH CDpa BDec is not totally similar to that of class II IMPDHs, this chimera shares the characteristic tetramer-octamer switch of class II IMPDHs. Similar observations were noted for the fourth chimera IMPDH CDpa BDbt (Table 3 and Extended data Fig. 6b), proving that the oligomeric state regulation is also transferred through the IMPDHbt Bateman domain.

To further confirm the different shapes and oligomeric states obtained by AUC in the different experimental conditions, we conducted small angle X-ray scattering (SAXS) experiments on the two chimeras IMPDH CDec BDpa and IMPDH CDpa BDec (Fig. 4b,e). Radii of gyration (R_g) and maximum particle dimension (d_{max}) calculated from Guinier plots and distance distribution P(r) functions (Extended data Fig. 7), and extracted molecular weight, are summarized in Extended data Table 2. Intensity scattering curves firstly showed similar curves for IMPDH CDec BDpa in the apo condition and in the presence of IMP (Fig. 4b) with identical local minimum. However, an upward or downward valley shift was

observed in the presence of NAD^+ or MgATP, respectively. Indeed, the intensity scattering curve in the presence of MgATP shows more pronounced peaks that are shifted in qR_g. This can be associated with more globular structures, in agreement with the results obtained by AUC. The distance distribution analysis reflects further these changes of shapes (Extended data Fig. 7). Nevertheless, dimensionless Kratky plots (Fig. 4c) show in all conditions double-bell shapes, a characteristic of well-folded globular multidomain proteins. In the case of IMPDH CDpa BDec, scattering curves present dissimilar features, with a notable presence of an accentuation of a smaller shoulder peak in the presence of NAD^+ or MgATP starting from qR_g values of 0.05 (Fig. 4e). Moreover, the addition of IMP yielded a curve with no valley. Like for the former chimera, dimensionless Kratky plots (Fig. 4f) show double-bell shapes, a characteristic of well-folded globular multidomain proteins, except in the presence of IMP to which an enlarged bell-shaped curve was obtained, indicating that the IMP-bound enzyme is in a highly compact form.

These experiments complemented our AUC data. IMPDH CDec BDpa is octameric in all conditions (MW around 400 kDa), while the IMPDH CDpa BDec is detected as an octamer in the apo condition (with the presence of a slight trace of tetramers that could not be further analyzed), a tetramer in the presence of IMP (MW around 200 kDa) and an octamer in the presence of MgATP. Additionally, it is clear that MgATP binding induces compaction of the overall structure in the case of both chimeras.

Altogether, our biophysical approaches validate a direct implication of the Bateman domain in the oligomeric state of the different IMPDHs.

Structural organization of IMPDH chimeras

Oligomeric state analysis prompted us to assess the structural characterization of IMPDH chimeras into more detail by X-ray crystallography and cryoelectronic microscopy (Cryo-

EM) single-particle analysis to correlate at the molecular level allosteric regulation transfer between class I and class II IMPDHs.

Crystals were only obtained for the chimera IMPDH CDec BDpa (Fig. 5a-c, Extended data Fig. 8a-k and Extended data Table 3). The best diffracting crystals afforded the determination of the 3D-structures of the apo form, and of the IMP- and MgATP-bound forms. A clear octameric organization is detected for all these structures by the PISA server[28]. The catalytic domains are clearly visible in all monomers while the Bateman domains are only partially visible. The first two structures (apo form and IMP-bound form) are highly similar, the only difference is the presence of visible IMP molecule in the catalytic domain of the structure of the IMP-bound IMPDH CDec BDpa while the remaining of the structure superimpose perfectly. These two structures adopt a flattened octamer as previously described[10] in the apo-form or inhibitor-bound form of other IMPDHs. On the contrary, the MgATP-bound form show a more spherical octameric architecture although not to the extent of the MnATP bound form of the wild-type IMPDHpa (PDB 4DQW). In agreement, two ATP molecules bind to each Bateman domain in a highly similar manner in both structures. This suggests that manganese was actually a good mimic for magnesium, and this allows matching the small magnesium cation in the electron density (Extended data Fig. 8g-h). In those two structures, the Bateman domains are more clearly visible suggesting that they are stabilized upon MgATP binding (Extended data Fig. 8i-k). The higher distances between the two tetramers formed by the catalytic domains within these octamers, lead to the melting of the flap region (residues 370-424) surrounding the active site. On the contrary, part of the electron density of these segments (residues 373-384 and 419-424) are visible in the two other structures (from crystals grown in the presence of IMP) and they bring additional contacts between the facing tetramers. Similar behaviors were already reported for IMPDHpa[17,29] and other IMPDHs once the conserved octameric organization was clearly established. Accordingly, the chimera

behaves very much like the wild-type enzyme sharing the same Bateman domain (Fig. 5d-f and Extended data Fig. 8d-f). Noteworthy, the structural changes observed at atomic resolution match the changes detected in solution by AUC and SAXS. This confirms that little crystal packing artifacts (if any) are at play here.

To get insights into the oligomeric state of the other chimera IMPDH CDpa BDec and its regulation by MgATP, we collected, after unsuccessful crystallization trials for this variant, cryo-EM data of the enzyme in the absence and presence of this nucleotide.

In the apo form (Fig. 6 and Extended data Table 4), we observed the dual presence of octameric and tetrameric species of the chimera. Fig. 6 shows crystallographic models fitted into the obtained 3D cryo-EM maps of the octamers (Fig. 6a-d) and tetramers (Fig. 6e-g) at 3.52 and 7.01 Å resolution, respectively. For both, the Bateman domains seem to be floppy and are only visible in some 2D and 3D classes corresponding to the octamers (Fig. 6a and Extended data Fig. 9). In contrast, in the presence of MgATP, only octameric particles were observed on grids for this chimera, and no tetramers were seen, as shown in the Extended data Fig. 10. In this state, the Bateman domains are clearly seen in the 2D classes. However, a severe problem of preferential orientation of the particles on the grids precluded us from obtaining high resolution maps.

Implication of the Bateman domain of IMPDH in *E. coli* physiology

Little is known about the physiological role of the conserved Bateman domain in prokaryotic IMPDHs. Previous work reported that a *guaB*$^{\Delta BD}$ *E. coli* strain harboring a genomic replacement of the sequence encoding the Bateman domain of IMPDHec by a 24-amino acid *scar* sequence showed a drastic deregulation of purine nucleotide pool[30]. This strain was also unable to grow in minimal medium supplemented with adenine or inosine[31]. To investigate the effect of our ΔBD and chimeric mutants on bacterial growth, we conducted

complementation assays using the *E. coli* Δ*guaB* strain from the Keio collection (JW5401)[32]. For that, we constructed pCmcI857 plasmids, in which each wild-type or mutant *guaB* gene was inserted under the control of the lambda pL promoter and its thermosensitive CmcI857 repressor (refer to Method for details). Hence, with this system, the expression of IMPDH (IMPDHec and IMPDHpa, the two corresponding ΔBD variants, and the two chimeras IMPDH CDec BDpa and IMPDH CDpa BDec) is induced by temperature-shift from 25°C to 37°C.

Since IMPDH is essential for survival in minimal medium, none of the JW5401 strains transformed with each pCmcI857 construct were able to grow at 25°C in M63B1 medium where there is no expression of the corresponding IMPDH. Then, we monitored bacterial growth of these strains at 37°C. As expected, the control strain transformed with an empty plasmid was not able to grow. On the other hand, bacterial growth was restored with all the other constructs, meaning that all IMPDH variants are expressed with a functional catalytic activity *in vivo* (Fig 7 and Extended data Fig. 11). Nevertheless, some variations between growth curves were noticeable. Strains complemented with IMPDHec or IMPDH CDpa BDec exhibited similar growth curves with calculated doubling time of 140 min. The bacteria that expressed IMPDHpa or IMPDH CDec BDpa, grew equally but slowly (doubling time 155 minutes) and their OD_{600} values for the stationary phase decreased compared to the cells encoding IMPDHs with a Bateman domain originating from IMPDHec. Intriguingly, ΔBD mutants exhibited non-homogenous pattern of the growth curves (Extended data Fig. 11).

Discussion

The Bateman domain[7], also known as a tandem-CBS motif, was shown to exist in multiple unrelated cytosolic or membrane proteins in all living organisms. Bateman domains were subsequently linked to regulatory functions[11,33] and several effectors[16,24] were then identified

as binding to CBS motifs, preponderantly adenosine nucleotides or derivatives, such as AMP[34,35], ADP[36-38], ATP[10,39], S-adenosyl methionine[40], diadenosine tetraphosphate[34] and cyclic di-AMP[41]. In addition, other nucleotides, as the example of the metabolic intermediate of purine *de novo* biosynthesis aminoimidazole carboxamide ribonucleotide (AICAR, also known as ZMP)[42], and magnesium ion[43], were also identified.

In this current study, we focused our interest on understanding the regulatory function of the Bateman domain of IMPDHs. In fact, we have previously shown that MgATP is an allosteric effector for IMPDH, and identified two canonical binding sites within the so-called Bateman domain[10]. Then the binding of nucleotides was extended to other IMPDHs[16,44]. We have concordantly shown that MgATP can activate the IMP-dehydrogenase activity or switch the homo-oligomeric state from a tetramer to an octamer, depending on the tested bacterial IMPDH, despite several reports claiming that all IMPDHs are exclusively tetrameric. As no known sequence signatures were identified in class I and class II IMPDHs to be linked to the molecular dichotomy between these two classes, in this present paper, we generated and characterized two types of variants: truncated forms that lost their own Bateman domain and chimeras that carry foreign Bateman domains.

Firstly, deleted forms of IMPDHs from the Bateman domain showed loss of MgATP-mediated regulation as expected. Additionally, ΔBD variants of IMPDHbt and IMPDHec were more active than their wild-type counterparts, illustrating an autoinhibitory property of the Bateman domain on reported IMPDHs. We previously showed similar observations on IMPDHpa and IMPDHpa ΔBD[10]. Early reports showed that the deletion of these modules from IMPDHec did not significantly affect the enzyme activity[30]. However, these observations were obtained by activity assays from soluble extracts of a *guaB*$^{\Delta BD}$ *E. coli* strain, and not from an overproduced and purified recombinant protein with protein concentration precisely determined. On the other hand, no effect of the Bateman domain

deletion on the catalytic properties were reported for human IMPDHs and IMPDH of *Ashbya gossypii*, illustrating inter-species variations[24,45].

Secondly, transplantation of allosteric regulation *via* permutation of Bateman domains between different bacterial IMPDHs showed MgATP-mediated allosteric regulation transfer. Interestingly, IMPDHs harboring a class II catalytic domain and a class I Bateman domain (IMPDH CDec BDpa and IMPDH CDbt BDpa) presented class I properties. The crystal structures of IMPDH CDec BDpa chimera showed at atomic level similar organization and structural rearrangements due to MgATP binding compared to IMPDHpa, which Bateman domain was derived from. This indicates that this domain is readily accommodated onto the catalytic domain from IMPDHec in agreement with the functional shift from a class-II to a class-I enzyme. This suggests a simple mechanism of regulation relying on extending the distance between the catalytic tetramers and subsequent local unfolding of the flap segments to activate the enzyme while little or no direct interplay between the catalytic and regulatory domains occurs. This correlates with the compaction observed upon MgATP binding. On the contrary, in the absence of the positive allosteric regulator, the class-I Bateman domains favor flattened octamers apparently limiting the flexibility of the active sites and therefore the entry and release of the substrates and products.

To get a clearer insight on the physiological role of the Bateman domain in bacterial IMPDHs, we evaluated the capacity of the mutants originating from IMPDHec and IMPDHpa in complementing a Δ*guaB E.* coli strain in minimal M63B1 medium, since bacteria can only rely on *de novo* synthesis of nucleotides and not the salvage pathway in these culture conditions, and therefore in need of IMPDH to finalize guanine nucleotide synthesis. Our results showed that deletion of the Bateman domain altered bacterial fitness. Chimera complementation showed similar growth rates for strains expressing an IMPDH

containing the same Bateman domain (wild-type or chimera). These observations suggest that the Bateman domain is an important component in IMPDH for optimal bacterial physiology.

From a fundamental point of view, several points are yet to be dissected. The molecular distinction between class I and class II IMPDHs is not very clear. Buey's group recently reported that IMPDHec and IMPDHpa are conjunctly inhibited in the presence of ATP and GTP/GDP[44]. Additionally, a new guanosine 5'-diphosphate 2'(3')-diphosphate (ppGpp) binding pocket was also identified in several class II IMPDHs[44]. These observations could suggest emerging evolutionary events that resulted in divergent allosteric regulation modes in bacterial IMPDHs.

The molecular importance of the ligand-induced oligomeric state switch in class II IMPDHs is also intriguing. Several eukaryotic and prokaryotic IMPDHs were shown to have DNA- and RNA-binding properties[25,46,47]. In the case of IMPDHec, binding of ATP to the Bateman domain inhibited binding to single stranded DNA[25]. IMPDH in eukaryotes and archaea was also shown to be capable of polymerizing into mesoscale homopolymers and heteropolymers (with CTP synthase), named cytoophidia[48,49]. Additionally, with a bacterial two hybrid approach, we recently screened for protein-protein interactions of all the enzymes implicated in purine *de novo* biosynthesis in *E. coli*. A dense network of binary interactions connecting most purine biosynthesis enzymes, including IMPDH, has been revealed[50]. Being implicated in pleiotropic associations within cells, it is tempting to speculate that oligomeric state switch of IMPDH could (de)favorize protein-protein or protein-nucleic acid interactions in response to cellular needs in metabolites, and therefore switching the enzyme between its metabolic function and other moonlighting functions.

Finally, in the optic of synthetic biology, our work can be also grouped to other successful attempts in extending the fundamental aspect of allostery to protein engineering applications, with aims to transfer allosteric regulations from a catalytic domain to another. For instance,

one study on 3-deoxy-D-arabino-heptulosonate 7-phosphate synthase, the enzyme catalyzing the first step of the shikimate pathway, aimed to generate a chimera comprised of the regulatory ACT domain of the ortholog of *Thermotoga maritima* to the $(ß/α)_8$-barrel catalytic domain of the unregulated ortholog *Pyrococcus furiosus* that naturally lacks the ACT domain[51]. This chimera exhibited a similar hydrodynamic shape and three-dimensional organization as the wild-type form of the ortholog of *T. maritima*. Transfer of enzymatic activity inhibition mediated by tyrosine and phenylalanine, two ligands of the ACT domain, was also observed[51]. Similarly, another example was reported with aspartate transcarbamylase, the enzyme catalyzing the first step of *de novo* pyrimidine biosynthesis: regulation transfer was observed from the characterization of a hybrid originating from a co-expression of the regulatory domain of ATP-activated ortholog of *E. coli* with the catalytic domain of the ATP-insensitive ortholog of *Erwinia herbicola*[52]. The same group subsequently identified one block of divergent residues implicated in effector-binding as being responsible for dictating ATP-sensitivity[53].

Overall, our work validates the Bateman domain as the carrier of the intrinsic molecular properties of both IMPDH classes and exemplifies that chimeragenesis strategies[54] could push the limits of synthetic biology for the design of novel enzymatic tools.

Materials and Methods

Cloning and construction of *guaB* variants

Plasmids used in this work are listed in Extended data Table 5 and the acronyms of corresponding expressed proteins are listed in Extended data Table 1. Sequences of cloning primers purchased from Eurofins MWG Operon are provided in Extended data Table 6. The

E. coli NM544 strain was used for molecular cloning. All recombinant ORFs were verified by DNA sequencing (Eurofins Genomics).

For the generation of ORFs encoding IMPDH variants devoid of the Bateman domain, site-directed mutagenesis was performed by PCR in two steps on plasmids pET28a-*guaBpa*, pET28a-*guaB*ec and pET28a-*guaB*bt using for each variant the T7 promotor and terminator primers and two mutant oligonucleotides as described previously for pET28a-*guaBpa*Δ*BD* for expression of IMPDHpa ΔBD[10].

For IMPDH chimeras, each ORF was generated by a three-step PCR procedure. First, each catalytic and Bateman domain was individually amplified with flanking complementary regions from pET28a plasmids containing the corresponding wild-type *guaB* genes. As the Bateman domain is inserted within the catalytic domain in the IMPDH primary sequence, it was necessary to amplify its coding sequence into two separate PCR products. Then, three PCR products (two corresponding to the catalytic domain and one to the Bateman domain) were ligated by a second PCR. A third and last PCR was used in the presence of Long T7 promotor and terminator primers to amplify the resulting full-length chimeric gene.

For constructs dedicated to protein production and purification, each corresponding ORF was cloned into pET28a plasmid (Novagen, Inc.) between the *Nde*I and *Hind*III restriction sites. *E. coli guaB* gene was amplified by PCR from *E. coli* K12 genomic DNA and was cloned into pET28a (noted pET28a-*guaBec*) as described previously for plasmids pET28a-*guaBpa* and pET28a-*guaBbt* (for expression of IMPDHpa and IMPDHbt respectively)[10,18].

In the case of the chimera IMPDH CDpa BDbt, the corresponding ORF was synthesized (with codon optimization for expression in *E. coli*) and directly inserted into pET28a by Twist Bioscience.

For bacterial complementation assays, the *Nde*I-*Aan*I DNA fragment containing wild-type or mutated *guaB* coding sequences from the corresponding pET28a plasmids were cloned into

an in-lab pCmcI857 plasmid digested by *Nde*I-*Sma*I. This plasmid allows to express a gene of interest under the transcriptional control of the heat-inducible pR promoter of λ bacteriophage. pCmcI857 was constructed by HiFi cloning assembly of the *Xho*I-*Hind*III fragment (p15A origin of replication, chloramphenicol resistance gene) from pZA35luc (Expressys) and a 893-bp PCR generated fragment from pDL1213[55] that contains the lambda pL/pR-cI857 expression system and a *Nde*I/*Kpn*I/*Pst*I/ *Sma*I/*BamH*I multicloning site.

Protein production and purification

All recombinant proteins were expressed as fusion proteins with a His-tag at the N-terminus in *E. coli* BL21(DE3)/pDIA17 strain[26] (except for IMPDHec and IMPDH CDpa BDbt, for which the expression was conducted in *E. coli* BL21 Star™ (DE3) (Thermo Fisher Scientific) or BL21 (DE3)/pGro7 (Chaperone BL21(DE3), TaKaRa Bio USA, Inc.) respectively). Bacteria transformed with the corresponding plasmid were grown at 37°C in 1 L of 2YT medium supplemented with 35 µg/ml kanamycin and 30 µg/ml chloramphenicol. Protein production was induced by adding 1 mM of IPTG to the growing culture. Bacteria were harvested by centrifugation after 3.5 hours of growth. In the case of IMPDHec, after induction with 1 mM IPTG, bacteria were grown at 30°C for 18 hours. In the case of IMDPH CDpa BDbt, protein production was induced with 0.5 mM IPTG, and bacteria were then grown at 16°C for 24 hours.

For purification, bacterial pellet was dissolved in the corresponding purification buffer (noted buffer A, see Extended data Table 1) supplemented with a cOmplete™ ULTRA EDTA-free protease inhibitor tablet (Roche Diagnostics) and lysed by sonication with a Bioblock Scientific Vibra Cell. After centrifugation at 10,000 g for one hour, the soluble fraction was added to a TALON metal affinity resin (TaKaRa Bio USA, Inc.). The further steps were

conducted as recommended by the manufacturer using the batch/gravity – flow purification procedure[56] at room temperature. Each protein was eluted with the corresponding purification buffer A supplemented with 150 mM imidazole. All eluted fractions were pooled and further purified by gel-filtration on a calibrated HiLoad™ 26/60 Superdex™ 200 prep grade (Cytiva Life Sciences) after prior equilibration with buffer A supplemented with 1 mM DTT and 1 mM EDTA.

Protein concentration was measured with the Bradford method[57], using a Bio-Rad kit, and by amino acid analysis on a Beckman system 6300 high-performance analyzer after acidic hydrolysis with 6 N HCl for 22 hours at 110°C. SDS-PAGE was performed as described by Laemmli[58]. Dynamic light scattering experiments were performed on a Dynapro plate reader (Wyatt technology) to verify sample homogeneity in corresponding buffer A and to search for more appropriate purification buffer when needed.

Enzymatic assay and kinetic characterization

Enzyme activity of each IMPDH variant was measured in a total volume of 0.5 mL of the corresponding optimal kinetics buffer (noted buffer K, see Extended data Table 1) at various concentrations of IMP and NAD^+, with or without 5 mM MgATP. After addition of IMPDH diluted in buffer K (final concentration range: 0.1 - 2 µM), initial velocity values were determined at 30°C on an Eppendorf ECOM 6122 photometer by monitoring the formation of NADH at 340 nm. Experimental data of at least three individual experiments were fitted using GraphPad Prism (GraphPad Prism Software, Inc.) and KaleidaGraph (Synergy Software, Inc.) according to the Michaelis-Menten equation (Eq. 1) or in the case of substrate inhibition at high substrate concentrations to equation 2 (Eq. 2), where v_0 is the initial reaction rate, V_m the maximum reaction rate, [S] the NAD^+ or IMP concentration, K_m the

Michaelis constant, and K_i the inhibitory constant. One unit of enzyme activity corresponds to 1 µmole of the product formed in 1 min.

$$v_0 = \frac{V_m[S]}{[S] + K_m} \quad (1)$$

$$v_0 = \frac{V_{max}[S]}{[S]\left(1+\frac{[S]}{K_i}\right) + K_m} \quad (2)$$

Analytical ultracentrifugation (AUC)

Sedimentation velocity experiments were performed at 20°C using a ProteomeLab XL-I (Beckman-Coulter) equipped with double-UV and Rayleigh interference detectors.

Samples were prepared in their corresponding buffer A supplemented with 0.5 mM of tris(2-carboxyethyl)phosphine within a total volume of 400 µL that was loaded to one of the two sectors of a 1.2 mm-thick two channels aluminum centerpiece of an epoxy cell with sapphire windows, the other sector being loaded with 420 µL of buffer free of effectors or proteins. The protein concentration was chosen between 0.1 and 3 mg/mL for the apo conditions, and at 1 mg/mL for the conditions in the presence of the different effectors (10 mM for IMP, 4 mM for NAD^+ or 5 mM for MgATP). Samples were spun at 30 000 rpm using an An-60 Ti rotor and 400 scans were obtained for each condition tested. Data analysis was conducted with Sedfit 12.0 using a continuous size distribution c(s) model to extract the sedimentation coefficient[59]. Sedimentation coefficients were corrected to standard conditions ($S_{20,w}$) and friction ratios (f/f_0) were calculated using Svedberg equation with the known molecular weights of each protein[60]. The estimation of the protein partial specific volume and corresponding buffer A viscosity and density (Extended data Table 7) was conducted with Sednterp 1.09 (available online from The Boston Biomedical Research Institute).

Size exclusion chromatography small-angle X-ray scattering (SEC-SAXS)

X-ray scattering was recorded after elution on a size exclusion column (Superose 6, 5 x 150 mm, Cytiva) on 1 mg/mL of each IMPDH variant supplemented with 6 mM IMP, 5 mM MgATP or 4 mM NAD^+ on the SWING beamline at Synchrotron SOLEIL (Saint-Aubin, France) and processed as previously described[10]. SAXS data collection parameters are listed in Extended data Table 8. Background-subtractions for intensity curves were conducted with FOXTROT. Data were then processed and analyzed using the program PRIMUS[61] from the ATSAS 3.0.5 software suite[62].

Crystallography and X-ray diffraction data collection

Crystallization condition screenings and hits optimization were performed at the Crystallography Core Facility of the Institut Pasteur[63]. Crystallization screens were carried out for two chimeras (IMPDH CDec BDpa and IMPDH CDpa BDec) using the sitting-drop vapor diffusion method using a MosquitoTM nanoliter-dispensing system (TTP Labtech). Reservoir solutions were 150 µL in volume and sitting drops were composed of 200 nL of protein (20 mg/mL) and 200 nL of reservoir solution, which was provided from different commercially accessible kits. The crystallization plates were stored at 18°C in a Rock-Imager1000® (Formulatrix) automated imaging system. For further optimizations, some of the conditions of interest were reproduced manually *via* the hanging drops method in Linbro plates. Diffracting crystals were only obtained for the chimera IMPDH CDec BDpa. Best crystals were obtained in the presence of 0.1 M Tris pH 8.5, 8% (w/v) PEG 8K and 1 mM IMP (PDB code 7QBJ); 0.05 M HEPES pH 7, 12% (w/v) PEG 3350, 1% tryptone, 0.001% NaN_3, and 10 mM IMP (PDB code 7QEM); or 10% (w/v) PEG 3K, 0.1 M NaCacod pH 6.5, 0.2 M $MgCl_2$, 5 mM MgATP, 4 mM NAD^+ (PDB code 7QDX). The collection of X-ray diffraction data from flash-cooled single crystals were conducted at Synchrotron SOLEIL, beamline Proxima 1 or 2A, (Saint-Aubin, France). Structures were solved by molecular

replacement using Phaser AutoMR[45] with previously published IMPDHpa structures (PDB 6GJV for the apo form[29] and PDB 4DQW MgATP-bound form[10]) as search probes. Model refinement was conducted with several types of refinement approaches using the current Python-based Hierarchical Environment for Integrated Crystallography (Phenix) software[64-66] and with alternating manual rebuilding in COOT[67]. Data processing and model refinement statistics are shown in Extended data Table 3. All structural figures were generated with the PyMol Molecular Graphics System, Version 1.3r1 (Schrödinger, LLC).

Cryo-EM sample preparation, data collection and image processing

4 µL of the chimera IMPDH CDpa BDec (0.7 mg/mL) in the absence or in the presence of 5 mM MgATP were applied onto 200 mesh CF-2/2-2CU-50 copper grids (Molecular Dimensions) that were plasma cleaned using Solarus II (Gatan). The samples were plunge-frozen using a Thermo Fisher Vitrobot Mark IV (Thermo Scientific®) at 4 °C, 100% humidity, and blotted for 3 seconds.

Cryo-EM data were collected on a Thermo-Fisher Glacios transmission electron microscope (Thermo Scientific®) operating at 200 keV. Micrographs were acquired with a Falcon 3 direct detector with a total electron exposure of 60 e−/Å^2 as a 42-frame dose-fractionated movie. The EPU data collection software was used to collect 1242 micrographs (0.96 Å/pixel) with a nominal defocus ranging from −0.8 µm to −2.4 µm.

Image processing was done in CryoSPARC[68]. Motion correction was performed using Patch Motion Correction. The contrast transfer function (CTF) parameters were estimated using Patch CTF estimation. A first particle picking done with the *blob picker* was used to generate 2D classes that were subsequently used as templates for template-based particles picking. Particles from 2D classes displaying high-resolution features were selected and used to generate reference-free 3D ab-initio models. The particles were further classified in 3D (see

Extended data Fig. 9). Final refinement steps imposing, either C4 or D4 symmetry, resulted in final reconstructions at ~ 7 and 3.6 Å resolution for the tetrameric and octameric forms, respectively (Extended data Fig. 9).

Bacterial complementation assay

For complementation analysis, growth behavior was analyzed in the *E. coli guaB* deleted strain (JW5401) from the Keio collection[32] transformed by different pCmcI857 constructs encoding IMPDH variants. Briefly, single colonies were inoculated and grown overnight in M63B1 (13.6 g/L potassium hydrogen phosphate, 0.2% ammonium sulfate, 0.01% magnesium sulfate, 0.025‰ iron sulfate, 0.002‰ thiamine hydrochloride, 0.2% glucose, pH 7) medium supplemented with 35 µg/ml kanamycin, 30 µg/ml chloramphenicol and 0.2% glucose. Bacterial suspension was then diluted to an initial optical density at 600 nm of 0.05 in 1 mL of the same medium culture at 37°C. Bacterial growth was monitored by measurement of optical density at 600 nm each 15 minutes with an automated UVmc1 spectrophotometer (SAFAS) equipped with a built-in thermostat and cuvette shaker.

Acknowledgements

This work was supported in part by the Centre National de la Recherche Scientifique (CNRS), the Institut National de la Santé Et de la Recherche Médicale (INSERM) and the Institut Pasteur. This work was also supported by the French Infrastructure for Integrated Structural Biology (FRISBI) ANR-10-INBS-0005. Antoine Gedeon and Nour Ayoub acknowledge PhD fellowships from the Médicament, Toxicologie, Chimie et Imageries Ph.D. school (MTCI, ED 563), Université Paris Cité.

We thank Jean-Marc Ghigo for providing the *E. coli* Δ*guaB* strain (JW5401) from the Keio collection. We also thank Pierre-Olivier Vidalain for advice in statistical analysis. We thank

Zakaria Jemouai for his participation in the optimization of protein expression and purification conditions. We thank Alexandre Chenal and Nicolas Wolf for fruitful discussions. The authors are grateful to the staff of the "Plate-Forme de Cristallographie" for robot-driven crystallization screening. We thank beamline scientists from the Synchrotron SOLEIL (St. Aubin, France) for advice in X-ray diffraction data collection on PROXIMA-1 and PROXIMA-2A beamlines, and SAXS data collection on SWING beamline. The NanoImaging Core at Institut Pasteur is acknowledged for support with sample preparation, image acquisition and analysis. The NanoImaging Core was created with the help of a grant from the French Government's Investissements d'Avenir program (EQUIPEX CACSICE - Centre d'analyse de systèmes complexes dans les environnements complexes, ANR-11-EQPX-0008). We acknowledge the staff from the Instruct Image Processing Center (I2PC) at the National Centre of Biotechnology-CSIC (Madrid) for support with cryo-EM image analysis.

Author contributions

A.G., G.L. and H.M.L. conceptualized and designed experiments; H.M.L. supervised the work; A.G. and G.K. performed cloning and site-directed mutagenesis; A.G. and N.A. provided purified proteins, accomplished biochemistry experiments and analyzed corresponding data; A.G. and S.B. conducted biophysical characterization and analyzed corresponding data; B.R. performed SAXS experiments and conducted the SAXS data analysis; A.G. and A.H. conducted crystallization; A.H. and A.M. collected X-ray data; M.G. and G.L. solved structures; A.M. prepared cryo-EM grids and performed image processing; A.G. and N.A. conducted bacterial complementation assays; A.G., G.L. and H.M.L. wrote the manuscript with input from all authors.

Data availability

The coordinate and structure factor files for IMPDH CDec BDpa have been deposited in the Protein Data Bank with accession code 7QBJ for the apo cform, 7QEM in complex with IMP and 7QDX in complex with MgATP. Other data are available from corresponding author upon request.

Competing interests

The authors declare no competing financial interests.

Additional information

Supplementary information refers to PDF file titled 'Supplementary Information'

Table 1. Steady-state kinetic parameters of IMPDH variants compared with wild-type forms, with IMP as variable substrate. Reaction rates were determined at a constant saturating concentration of NAD^+ (3 mM for IMPDH CDpa BDec; 4 mM for IMPDHec ΔBD, IMPDHbt ΔBD and IMPDH CDec BDpa; 5 mM for IMPDHec and IMPDH CDbt BDpa) and in the absence or presence of 5 mM MgATP. The experimental data were fitted according to the Michaelis-Menten equation (see Materials and Methods).

	In the absence of MgATP		In the presence of MgATP	
	V_m (U/mg)	K_m^{IMP} (μM)	V_m (U/mg)	K_m^{IMP} (μM)
IMPDHec	5.55 ± 0.09	32 ± 7	5.54 ± 0.08	31 ± 6
IMPDHec ΔBD	12.52 ± 0.33	35 ± 10	12.31 ± 0.39	59 ± 11
IMPDHbt*	2.56 ± 0.04	52 ± 4	2.52 ± 0.12	39 ± 9
IMPDHbt ΔBD	6.42 ± 0.11	35 ± 7	7.17 ± 0.18	52 ± 10
IMPDHpa**	2.13 ± 0.07	1760 ± 109	5.58 ± 0.21	36 ± 4
IMPDHpa ΔBD**	5.75 ± 0.11	34 ± 2	4.78 ± 0.07	24 ± 2
IMPDH CDec BDpa	3.58 ± 0.10	239 ± 3	3.84 ± 0.10	52 ± 11
IMPDH CDbt BDpa	1.56 ± 0.08	106 ± 30	6.43 ± 0.45	42 ± 13
IMPDH CDpa BDec	5.22 ± 0.15	89 ± 19	5.26 ± 0.12	96 ± 15
IMPDH CDpa DBbt	6.62 ± 0.17	51 ± 13	6.99 ± 0.14	64 ± 10

IMPDHpa exhibits positive cooperativity towards IMP in the absence of MgATP: in this case, the data were fitted to the Hill equation, thus instead of the Michaelis constant K_m, the half-maximal concentration constant is noted $K_{0.5}$.

*Data taken from Alexandre *et al.*[18]; ** data taken from Labesse *et al.*[10].

Table 2. Steady-state kinetic parameters of IMPDH variants compared with corresponding wild-type forms, with NAD^+ as variable substrate. Reaction rates were determined at a constant saturating concentration of IMP (2 mM for IMPDH CDbt BDpa; 3 mM for IMPDH CDpa BDec; 4 mM for IMPDHec ΔBD, IMPDHbt ΔBD and IMPDH CDec BDpa; 5 mM for IMPDHec) and in the absence or presence of 5 mM MgATP. The experimental data were fitted according to the Michaelis-Menten or the substrate inhibition equation (see Materials and Methods).

	In the absence of MgATP			In the presence of MgATP		
	V_m (U/mg)	K_m^{NAD} (μM)	K_i^{NAD} (μM)	V_m (U/mg)	K_m^{NAD} (μM)	K_i^{NAD} (μM)
IMPDHec	6.77 ± 0.50	578 ± 131	N.A.	6.68 ± 0.50	692 ± 155	N.A.
IMPDHec ΔBD	26.50 ± 1.40	1937 ± 227	N.A.	22.65 ± 1.34	2209 ± 270	N.A.
IMPDHbt*	2.82 ± 0.07	355 ± 27	4800 ± 1430	2.78 ± 0.14	418 ± 60	N.A.
IMPDHbt ΔBD	10.94 ± 1.09	741 ± 132	7498 ± 2103	13.32 ± 2.33	1231 ± 310	4150 ± 1464
IMPDHpa**	2.26 ± 0.07	139 ± 14	N.A.	9.00 ± 0.50	498 ± 44	4067 ± 550
IMPDHpa ΔBD**	10.40 ± 0.50	580 ± 47	4445 ± 566	8.85 ± 0.83	499 ± 78	3967 ± 912
IMPDH CDec BDpa	4.65 ± 0.40	2257 ± 437	N.A.	4.84 ± 0.21	645 ± 95	N.A.
IMPDH CDbt BDpa	2.24 ± 0.50	117 ± 99	2363 ± 1112	6.30 ± 0.37	487 ± 111	N.A.
IMPDH CDpa BDec	6.10 ± 0.20	464 ± 52.8	N.A.	6.38 ± 0.27	494 ± 69	N.A.
IMPDH CDpa DBbt	9.11 ± 0.25	783 ± 65	N.A.	8.80 ± 0.40	897 ± 119	N.A.

*Data taken from Alexandre *et al.*[18]; ** data taken from Labesse *et al.*[10].
N.A.: not applicable.

Table 3. AUC data for ΔBD and chimeras of IMPDHs tested at 1 mg/mL.

*: higher-order species are also present; **: an intermediate species is also present.

		$S_{20,w}$ (S)	f/f_0	Oligomeric state
IMPDHec ΔBD	**Apo**	9.1 and 11.7	1.20 and 1.45	Tetramer and octamer
	IMP	8.1	1.30	Tetramer
	NAD^+	10.4	1.05	Tetramer
	MgATP	7.8	1.35	Tetramer
IMPDHbt ΔBD	**Apo**	7.9	1.35	Tetramer
	IMP	8.7	1.25	Tetramer
	NAD^+	8.6	1.25	Tetramer
	MgATP	7.8	1.45	Tetramer
IMPDH CDec BDpa	**Apo**	14.5	1.35	Octamer
	IMP	14.1	1.40	Octamer
	NAD^+	14.2	1.40	Octamer
	MgATP	15.0	1.30	Octamer
IMPDH CDbt BDpa	**Apo**	13.7	1.45	Octamer
	IMP	13.5	1.45	Octamer
	NAD^+	13.1	1.50	Octamer
	MgATP	14.2	1.40	Octamer
IMPDH CDpa BDec	**Apo**	8.9 and 13.1	1.40 and 1.50	Tetramer and octamer*
	IMP	7.8	1.60	Tetramer
	NAD^+	7.4 and 13.2	1.70 and 1.50	Tetramer and octamer**
	MgATP	14.5	1.35	Octamer
IMPDH CDpa DBbt	**Apo**	9.9 and 12.9	1.25 and 1.50	Tetramer and octamer
	IMP	8.6	1.45	Tetramer
	NAD^+	13.7	1.40	Octamer
	MgATP	13.9	1.35	Octamer

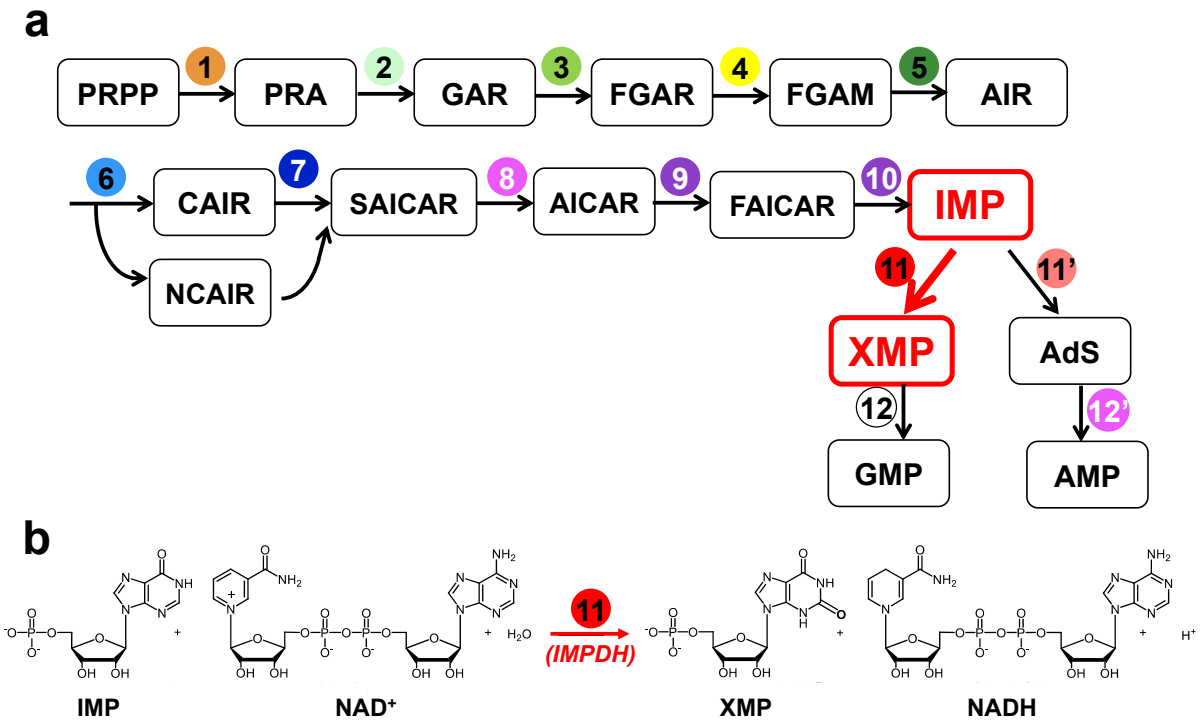

Fig. 1: Position of IMPDH in *de novo* purine biosynthesis. (**a**) *De novo* purine biosynthetic pathway consists of 14 conserved chemical steps numbered from 1 to 12'. In bacteria, enzymes involved in this pathway are PurF ( ), PurD ( ), PurN or PurT ( ), PurL ( ), PurM ( ), PurK and PurE ( ), PurC ( ), PurB (and), PurH ( ), IMPDH ( ), GuaB ( ) and PurA ( ).

(**b**) Reaction catalyzed by IMPDH.

Abbreviations of metabolites are defined as followed: PRPP, 5-phosphoribosyl-1-pyrophosphate; PRA, 5-phosphoribosyl-1-amine ; GAR, 5'-phosphoribosylglycinamide; FGAR, 5'-phosphoribosyl-N-formylglycinamide; FGAM, 5'-phosphoribosyl-N-formyl glycineamidine; AIR, 5-aminoimidazole ribonucleotide; NCAIR,; N5-carboxyamino-imidazole ribonucleotide; CAIR, 5-phosphoribosyl-4-carboxy-5-aminoimidazole; SAICAR, 5-Amino-4-imidazole-N-succinocarboxamide ribonucleotide; AICAR, 5-aminoimidazole-4-carboxamide ribonucleotide; FAICAR, 5-formamidoimidazole-4-carboxamide ribonucleotide; IMP, inosine 5'-monophosphate; NAD^+/NADH, nicotinamide adenine dinucleotide; XMP, xanthosine 5'-monophosphate; GMP, guanosine 5'-monophosphate; AdS, adenylosuccinate; AMP, adenosine 5'-monophosphate.

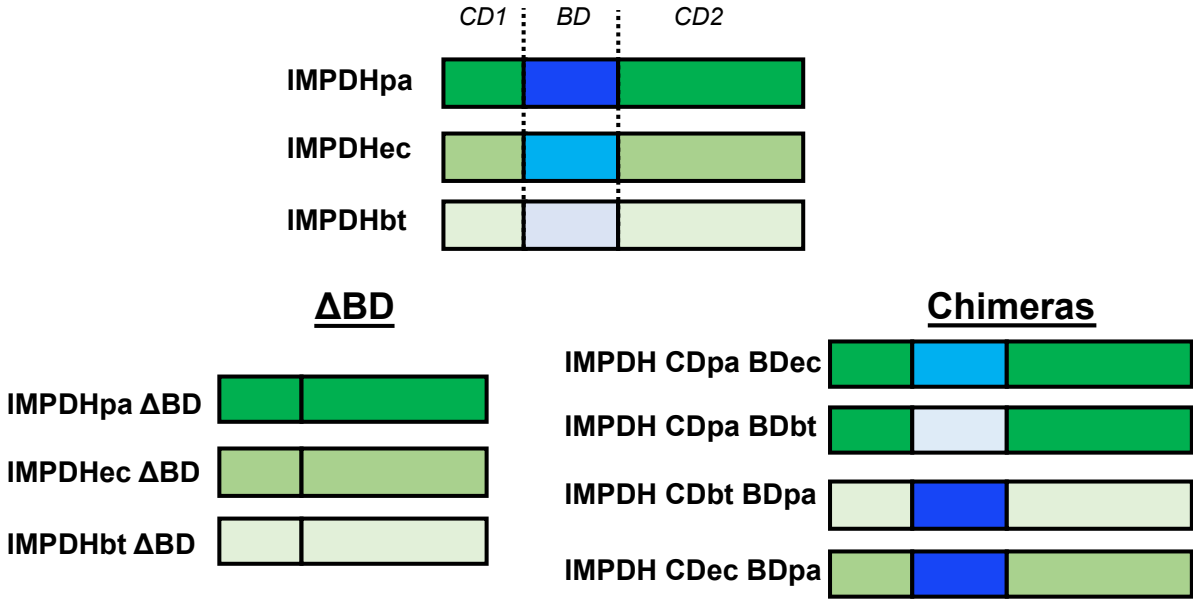

Fig. 2: Schematic overview of generated IMPDH variants. From the three considered parent enzymes (IMPDH of *P. aeruginosa*, *E. coli* and *B. thailandensis* noted IMPDHpa, IMPDHec and IMPDHbt, respectively), deleted forms from the Bateman domain (ΔBD) and chimeras were generated. The catalytic domain (CD) is colored in green, the Bateman domain (BD) in blue.

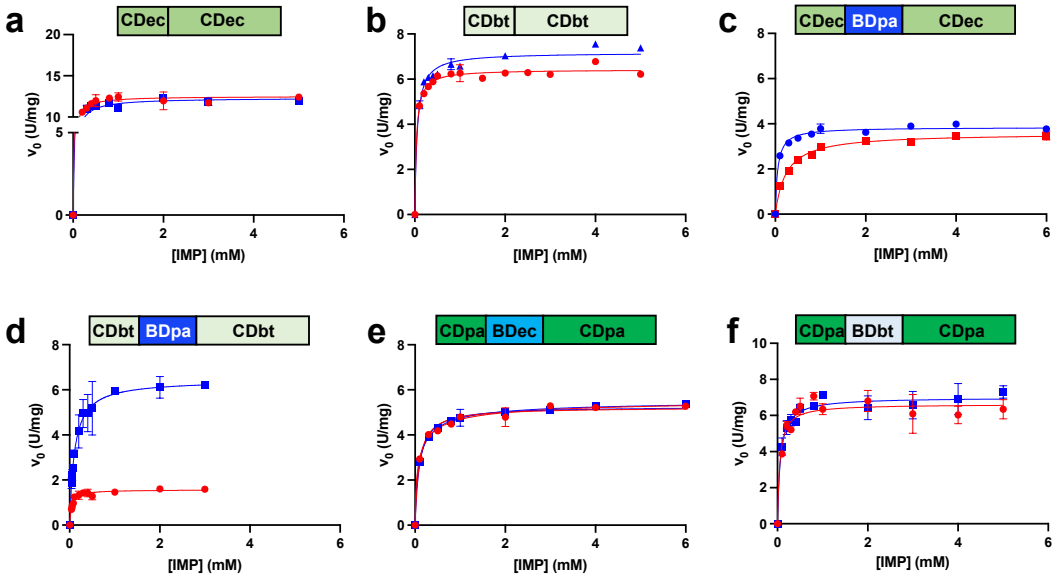

Fig. 3: Bateman domain deletion or permutation's effect on IMPDH kinetic regulation by MgATP. The order of the enzymes is as follows: (**a**) IMPDHec ΔBD, (**b**) IMPDHbt ΔBD, (**c**) IMPDH CDec BDpa, (**d**) IMPDH CDbt BDpa, (**e**) IMPDH CDpa BDec, (**f**) IMPDH CDpa BDbt. The variation of the initial velocity as a function of variable concentrations of the substrate IMP is plotted in the absence (in red) or in the presence (in blue) of 5 mM MgATP. Saturating concentrations of NAD^+ were as followed: 4 mM for IMPDHec ΔBD, IMPDHbt ΔBD and IMPDH CDec BDpa; 3 mM for IMPDH CDpa BDec and IMPDH CDpa BDbt; and 5 mM for IMPDH CDbt BDpa. Plots were fitted according to the Michaelis-Menten equation and error-bars represent standard deviation of at least three independent measurements.

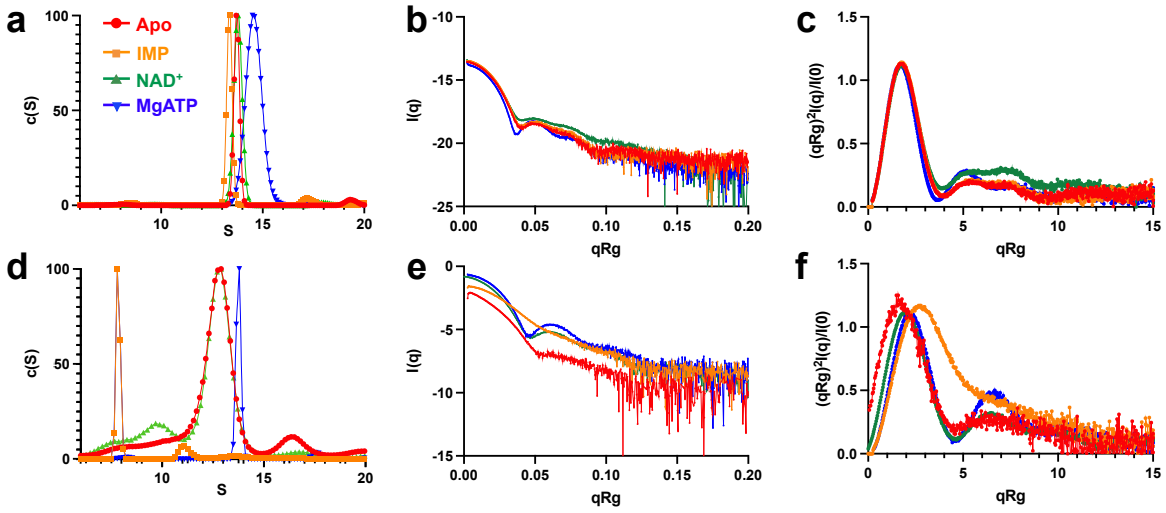

Fig. 4: IMPDH chimera oligomeric state regulation in the presence of different ligands. Upper lane (**a-c**) and lower lane (**d-f**) correspond for IMPDH CDec BDpa and IMPDH CDpa BDec data, respectively. (**a**) and (**d**), AUC continuous sedimentation coefficient c(S) distribution in the absence or in the presence of 10 mM IMP, 4 mM NAD^+, or 5 mM MgATP. The concentration of protein was fixed at 1 mg/mL. Sedimentation coefficients are expressed in Svedberg units (1S = 10^{-13} s).
(**b-c** and **e-f**), Experimental SAXS scattering intensity curves (**b**,**e**) and dimensionless Kratky plots (**c**,**f**). Proteins were injected at a concentration of 6.5 mg/mL for IMPDH CDec BDpa and 7 mg/mL for IMPDH CDpa BDec in apo condition or in the presence of 6 mM IMP, 4 mM NAD^+ or 5 mM MgATP. Data (**a-f**) for the apo condition or in the presence of IMP, NAD^+ or MgATP are colored in red, orange, green and blue, respectively.

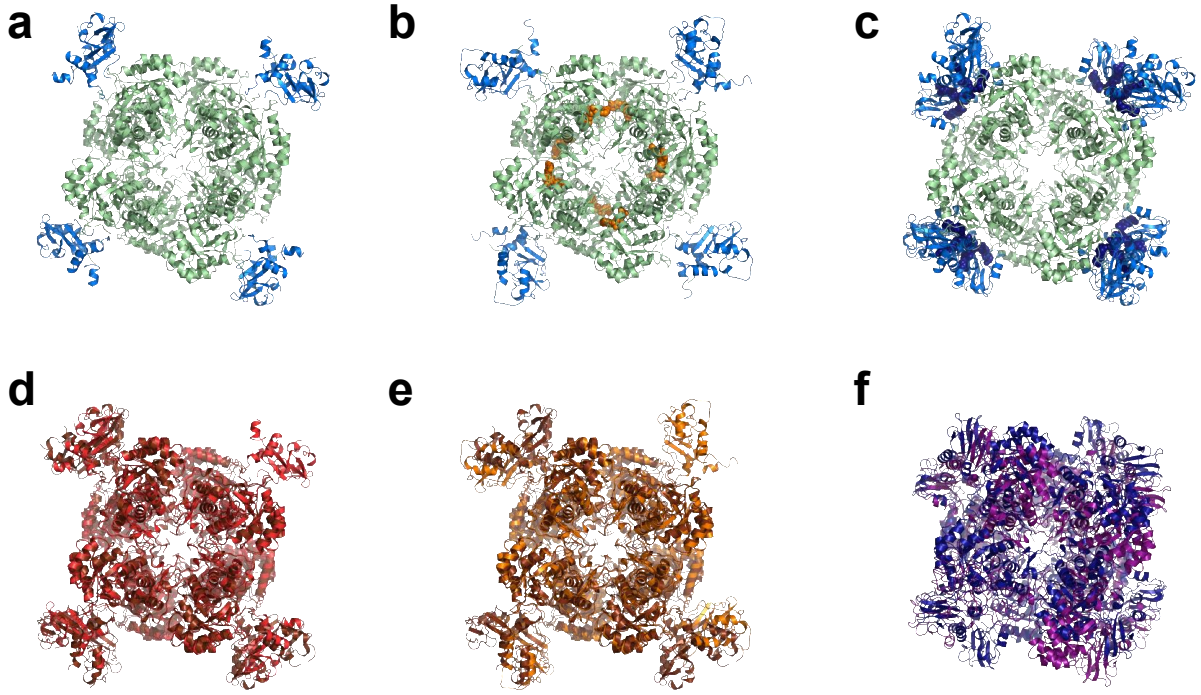

Fig. 5: X-ray structures of the IMPDH CDec BDpa chimera (a-c) and comparison with the previously published structures of the wild-type IMPDHpa structures (d-f).
(**a**) apo form, (**b**) in the presence of IMP or (**c**) in the presence of MgATP. The polypeptide chains (catalytic domains in green and Bateman domains in blue) are shown as ribbons. IMP molecules, each bound to the catalytic sites, are shown as orange spheres. MgATP molecules, each bound to the Bateman domains are shown as dark blue spheres. For both ligands, there is a full occupancy of the binding-sites. (**d**) Superimposition of the structures of the apo forms of the IMPDH CDec BDpa chimera (shown in red) and the wild-type IMPDHpa (shown in bronze; PDB code 6GJV[29]). (**e**) Superimposition of the structures of IMPDH CDec BDpa chimera in complex with IMP (shown in orange) and the wild-type IMPDHpa (shown in bronze; PDB code 6GJV[29]). (**f**) Superimposition of the structures of the IMPDH CDec BDpa chimera (shown in blue) and the wild-type IMPDHpa (shown in purple; PDB code 4DQW[10]) in complex with MgATP.

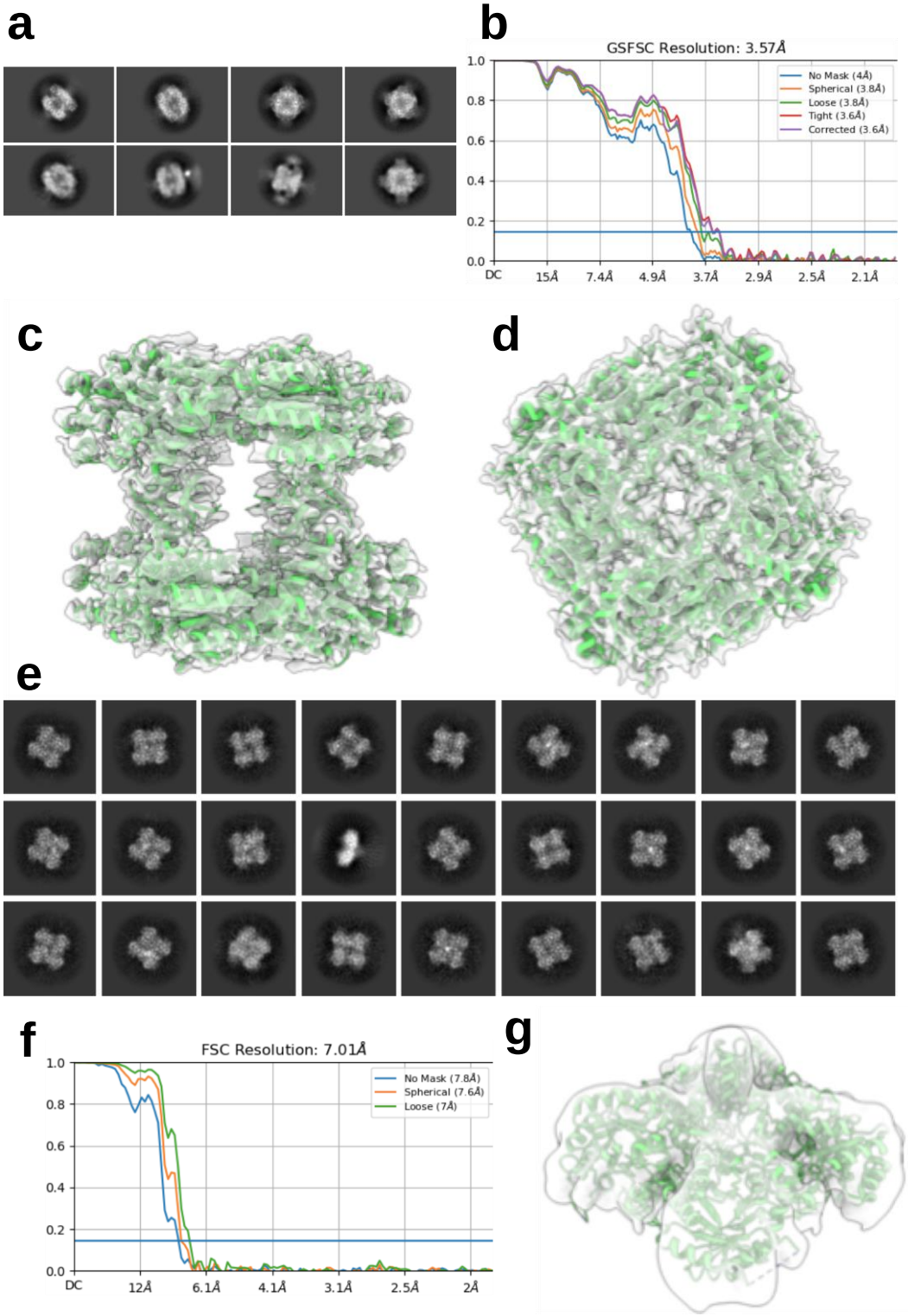

Fig. 6: Cryo-EM data of particles of the IMPDH CDpa BDec apo form.
(**a-d**) Data of octameric population. (**a**) Representative 2D classes of octamers with (**b**) the corresponding Fourier shell correlation (FSC) curves and (**c-d**) 3D density reconstruction. (**e-g**) Data of tetrameric population. (**e**) Representative 2D classes of tetramers. (**f**) FSC curves corresponding to the cryo-EM map shown in (**g**). The catalytic domain is represented in

green. Crystallographic models of IMPDHpa (PDB 6GJV) were fitted into the 3D maps of octamer (**c,d**) and tetramer (**g**).

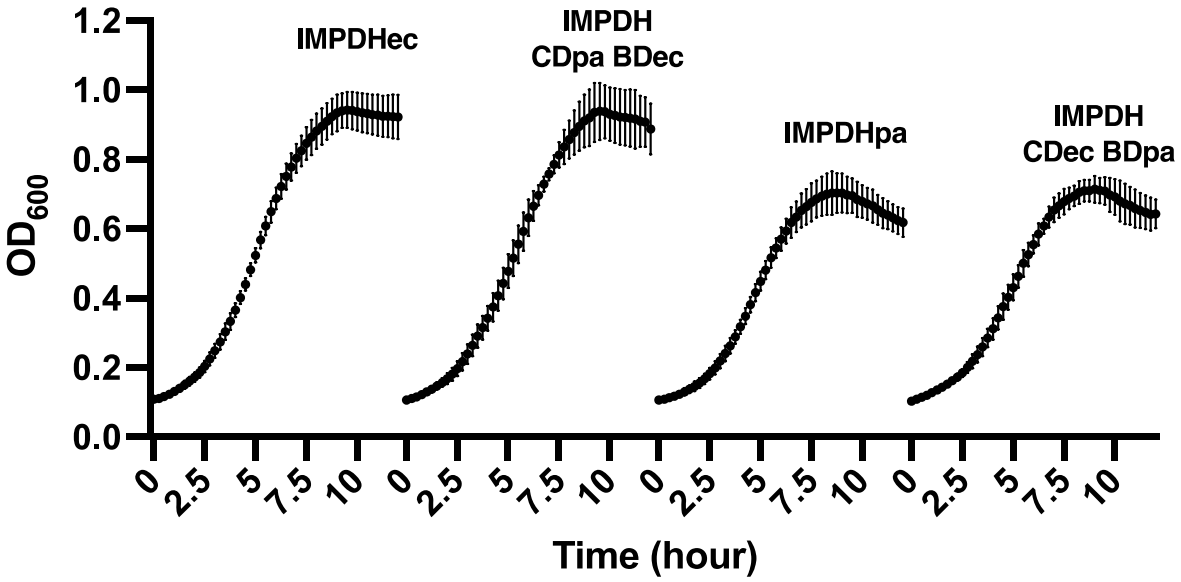

Fig. 7: Growth curves in M63B1 medium at 37°C of JW5401 strains transformed with different pCmcI857 constructs encoding wild-type or chimeric IMPDHs. Optical density was measured at 600 nm every 15 minutes for 12h. For each strain (expressing either wild-type IMPDHec, IMPDH CDpa BDec, wild-type IMPDHpa or IMPDH CDec BDpa as indicated above the curves), mean data curves are shown, with error bars representing standard deviation of five independent experiments.

References

1. Gebauer F, Hentze MW. Molecular mechanisms of translational control. *Nat Rev Mol Cell Biol.* 2004;5(10):827-835.
2. Chothia C, Gough J, Vogel C, Teichmann SA. Evolution of the protein repertoire. *Science.* 2003;300(5626):1701-1703.
3. Changeux JP. Allostery and the Monod-Wyman-Changeux model after 50 years. *Annual Rev Biophys.* 2012;41:103-133.
4. Changeux JP. 50 years of allosteric interactions: the twists and turns of the models. *Nat Rev Mol Cell Biol.* 2013;14(12):819-829.
5. Monod J, Wyman J, Changeux JP. On the Nature of Allosteric Transitions: a Plausible Model. *J Mol Biol.* 1965;12:88-118.
6. Koshland DE, Jr., Nemethy G, Filmer D. Comparison of experimental binding data and theoretical models in proteins containing subunits. *Biochemistry.* 1966;5(1):365-385.
7. Bateman A. The structure of a domain common to archaebacteria and the homocystinuria disease protein. *Trends Biochem Sci.* 1997;22(1):12-13.
8. Hedstrom L. IMP dehydrogenase: structure, mechanism, and inhibition. *Chem Rev.* 2009;109(7):2903-2928.
9. Zhou X, Cahoon M, Rosa P, Hedstrom L. Expression, Purification, and Characterization of Inosine 5′-Monophosphate Dehydrogenase from *Borrelia burgdorferi*. *J Biol Chem.* 1997;272(35):21977-21981.
10. Labesse G, Alexandre T, Vaupré L, et al. MgATP Regulates Allostery and Fiber Formation in IMPDHs. *Structure.* 2013;21(6):975-985.
11. Ignoul S, Eggermont J. CBS domains: structure, function, and pathology in human proteins. *Am J Physiol Cell Physiol.* 2005;289(6):C1369-C1378.
12. Bowne SJ, Sullivan LS, Blanton SH, et al. Mutations in the inosine monophosphate dehydrogenase 1 gene (IMPDH1) cause the RP10 form of autosomal dominant retinitis pigmentosa. *Hum Mol Genet.* 2002;11(5):559-568.
13. Bowne SJ, Sullivan LS, Mortimer SE, et al. Spectrum and Frequency of Mutations in IMPDH1 Associated with Autosomal Dominant Retinitis Pigmentosa and Leber Congenital Amaurosis. *Invest Ophthalmol Vis Sci.* 2006;47(1):34-42.
14. Kennan A, Aherne A, Palfi A, et al. Identification of an IMPDH1 mutation in autosomal dominant retinitis pigmentosa (RP10) revealed following comparative microarray analysis of transcripts derived from retinas of wild-type and Rho–/– mice. *Human Molecular Genetics.* 2002;11(5):547-558.
15. Anashkin VA, Baykov AA, Lahti R. Enzymes Regulated via Cystathionine beta-Synthase Domains. *Biochemistry (Mosc).* 2017;82(10):1079-1087.
16. Ereño-Orbea J, Oyenarte I, Martinez-Cruz LA. CBS domains: Ligand binding sites and conformational variability. *ArchBiochem Biophys.* 2013;540(1-2):70-81.
17. Labesse G, Alexandre T, Gelin M, Haouz A, Munier-Lehmann H. Crystallographic studies of two variants of *Pseudomonas aeruginosa* IMPDH with impaired allosteric regulation. *Acta Crystallographica Section D.* 2015;71(9):1890-1899.
18. Alexandre T, Raynal B, Munier-Lehmann H. Two classes of bacterial IMPDHs according to their quaternary structures and catalytic properties. *PLoS ONE.* 2015;10(2):e0116578.
19. Buey RM, Fernandez-Justel D, Marcos-Alcalde I, et al. A nucleotide-controlled conformational switch modulates the activity of eukaryotic IMP dehydrogenases. *Sci Rep.* 2017;7(1):2648.

20. Buey RM, Fernandez-Justel D, Jimenez A, Revuelta JL. The gateway to guanine nucleotides: Allosteric regulation of IMP dehydrogenases. *Protein Sci.* 2022;31(9):e4399.
21. Anthony SA, Burrell AL, Johnson MC, et al. Reconstituted IMPDH polymers accommodate both catalytically active and inactive conformations. *Mol Biol Cell.* 2017;28(20):2600-2608.
22. Burrell AL, Nie C, Said M, et al. IMPDH1 retinal variants control filament architecture to tune allosteric regulation. *Nat Struct Mol Biol.* 2022;29(1):47-58.
23. Powell G, Rajagopalan KV, Handler P. Purification and Properties of Inosinic Acid Dehydrogenase from *Escherichia coli*. *Journal of Biological Chemistry.* 1969;244(17):4793-4797.
24. Buey RM, Ledesma-Amaro R, Velazquez-Campoy A, et al. Guanine nucleotide binding to the Bateman domain mediates the allosteric inhibition of eukaryotic IMP dehydrogenases. *Nat Commun.* 2015;6:8923.
25. Despotovic D, Brandis A, Savidor A, Levin Y, Fumagalli L, Tawfik DS. Diadenosine tetraphosphate (Ap4A) - an *E. coli* alarmone or a damage metabolite? *FEBS J.* 2017;284(14):2194-2215.
26. Munier H, Gilles A-M, Glaser P, et al. Isolation and characterization of catalytic and calmodulin-binding domains of *Bordetella pertussis* adenylate cyclase. *Eur J Biochem.* 1991;196:469-474.
27. de Marco A, Berrow N, Lebendiker M, et al. Quality control of protein reagents for the improvement of research data reproducibility. *Nat Commun.* 2021;12(1):2795.
28. Krissinel E, Henrick K. Inference of Macromolecular Assemblies from Crystalline State. *Journal of Molecular Biology.* 2007;372(3):774-797.
29. Alexandre T, Lupan A, Helynck O, et al. First-in-class allosteric inhibitors of bacterial IMPDHs. *Eur J Med Chem.* 2019;167:124-132.
30. Pimkin M, Markham GD. The CBS subdomain of inosine 5′-monophosphate dehydrogenase regulates purine nucleotide turnover. *Mol Microbiol.* 2008;68(2):342-359.
31. Pimkin M, Pimkina J, Markham GD. A regulatory role of the Bateman domain of IMP dehydrogenase in adenylate nucleotide biosynthesis. *J Biol Chem.* 2009;284(12):7960-7969.
32. Baba T, Ara T, Hasegawa M, et al. Construction of *Escherichia coli* K-12 in-frame, single-gene knockout mutants: the Keio collection. *Mol Syst Biol.* 2006;2:2006 0008.
33. Baykov AA, Tuominen HK, Lahti R. The CBS Domain: A Protein Module with an Emerging Prominent Role in Regulation. *ACS Chemical Biology.* 2011;6(11):1156-1163.
34. Tuominen H, Salminen A, Oksanen E, et al. Crystal structures of the CBS and DRTGG domains of the regulatory region of *Clostridium perfringens* pyrophosphatase complexed with the inhibitor, AMP, and activator, diadenosine tetraphosphate. *J Mol Biol.* 2010;398(3):400-413.
35. Xiao B, Heath R, Saiu P, et al. Structural basis for AMP binding to mammalian AMP-activated protein kinase. *Nature.* 2007;449(7161):496-500.
36. Jin X, Townley R, Shapiro L. Structural insight into AMPK regulation: ADP comes into play. *Structure.* 2007;15(10):1285-1295.
37. Meyer S, Savaresi S, Forster IC, Dutzler R. Nucleotide recognition by the cytoplasmic domain of the human chloride transporter ClC-5. *Nat Struct Mol Biol.* 2007;14(1):60-67.
38. Xiao B, Sanders MJ, Underwood E, et al. Structure of mammalian AMPK and its regulation by ADP. *Nature.* 2011;472(7342):230-233.

39. Imamura A, Okada T, Mase H, et al. Allosteric regulation accompanied by oligomeric state changes of Trypanosoma brucei GMP reductase through cystathionine-beta-synthase domain. *Nat Commun.* 2020;11(1):1837.
40. Majtan T, Pey AL, Fernandez R, Fernandez JA, Martinez-Cruz LA, Kraus JP. Domain organization, catalysis and regulation of eukaryotic cystathionine beta-synthases. *PLoS One.* 2014;9(8):e105290.
41. Huynh TN, Choi PH, Sureka K, et al. Cyclic di-AMP targets the cystathionine beta-synthase domain of the osmolyte transporter OpuC. *Mol Microbiol.* 2016;102(2):233-243.
42. Day P, Sharff A, Parra L, et al. Structure of a CBS-domain pair from the regulatory gamma1 subunit of human AMPK in complex with AMP and ZMP. *Acta Crystallogr D Biol Crystallogr.* 2007;63(Pt 5):587-596.
43. Hattori M, Tanaka Y, Fukai S, Ishitani R, Nureki O. Crystal structure of the MgtE Mg2+ transporter. *Nature.* 2007;448(7157):1072-1075.
44. Fernandez-Justel D, Marcos-Alcalde I, Abascal F, et al. Diversity of mechanisms to control bacterial GTP homeostasis by the mutually exclusive binding of adenine and guanine nucleotides to IMP dehydrogenase. *Protein Sci.* 2022;31(5):e4314.
45. Nimmesgern E, Black J, Futer O, et al. Biochemical analysis of the modular enzyme inosine 5'-monophosphate dehydrogenase. *Protein Expr Purif.* 1999;17(2):282-289.
46. Cornuel JF, Moraillon A, Guéron M. Participation of yeast inosine 5′-monophosphate dehydrogenase in an in vitro complex with a fragment of the C-rich telomeric strand. *Biochimie.* 2002;84(4):279-289.
47. McLean JE, Hamaguchi N, Belenky P, Mortimer SE, Stanton M, Hedstrom L. Inosine 5'-monophosphate dehydrogenase binds nucleic acids in vitro and in vivo. *Biochem J.* 2004;379:243-251.
48. Calise SJ, Purich DL, Nguyen T, et al. 'Rod and ring' formation from IMP dehydrogenase is regulated through the one-carbon metabolic pathway. *J Cell Sci.* 2016;129(15):3042-3052.
49. Fernandez-Justel D, Nunez R, Martin-Benito J, et al. A Nucleotide-Dependent Conformational Switch Controls the Polymerization of Human IMP Dehydrogenases to Modulate their Catalytic Activity. *J Mol Biol.* 2019;431(5):956-969.
50. Gedeon A, Karimova G, Ayoub N, et al. Interaction network among *de novo* purine nucleotide biosynthesis enzymes in *Escherichia coli*. *FEBS J.* 2023.
51. Cross PJ, Allison TM, Dobson RC, Jameson GB, Parker EJ. Engineering allosteric control to an unregulated enzyme by transfer of a regulatory domain. *Proc Natl Acad Sci U S A.* 2013;110(6):2111-2116.
52. Wales ME, Madison LL, Glaser SS, Wild JR. Divergent allosteric patterns verify the regulatory paradigm for aspartate transcarbamylase. *J Mol Biol.* 1999;294(5):1387-1400.
53. Cunin R, Rani CS, Van Vliet F, Wild JR, Wales M. Intramolecular signal transmission in enterobacterial aspartate transcarbamylases II. Engineering co-operativity and allosteric regulation in the aspartate transcarbamylase of *Erwinia herbicola*. *J Mol Biol.* 1999;294(5):1401-1411.
54. Balabanova L, Golotin V, Podvolotskaya A, Rasskazov V. Genetically modified proteins: functional improvement and chimeragenesis. *Bioengineered.* 2015;6(5):262-274.
55. Ladant D. Calcium and membrane binding properties of bovine neurocalcin delta expressed in Escherichia coli. *J Biol Chem.* 1995;270(7):3179-3185.
56. TALON® Metal Affinity Resins User Manual. In. Vol PT1320-1 (PR34731): BD Biosciences; 2003.

57. Bradford MM. A rapid and sensitive method for the quantitation of microgram quantities of protein utilizing the principle of protein-dye-binding. *Anal Biochem.* 1976;72:248-254.
58. Laemmli UK. Cleavage of structural proteins during the assembly of the head of bacteriophage T4. *Nature* 1970;227:680-685.
59. Solovyova A, Schuck P, Costenaro L, Ebel C. Non-Ideality by Sedimentation Velocity of Halophilic Malate Dehydrogenase in Complex Solvents. *Biophysical Journal.* 2001;81(4):1868-1880.
60. Correia JJ, Stafford WF. Sedimentation Velocity: A Classical Perspective. *Methods Enzymol.* 2015;562:49-80.
61. Konarev PV, Volkov VV, Sokolova AV, Koch MHJ, Svergun DI. PRIMUS: a Windows PC-based system for small-angle scattering data analysis. *J Appl Cryst.* 2003;36(5):1277-1282.
62. Manalastas-Cantos K, Konarev PV, Hajizadeh NR, et al. ATSAS 3.0: expanded functionality and new tools for small-angle scattering data analysis. *J Appl Crystallogr.* 2021;54(Pt 1):343-355.
63. Weber P, Pissis C, Navaza R, et al. High-Throughput Crystallization Pipeline at the Crystallography Core Facility of the Institut Pasteur. *Molecules.* 2019;24(24).
64. Afonine PV, Mustyakimov M, Grosse-Kunstleve RW, Moriarty NW, Langan P, Adams PD. Joint X-ray and neutron refinement with phenix.refine. *Acta Crystallogr D Biol Crystallogr.* 2010;66(Pt 11):1153-1163.
65. Burnley BT, Afonine PV, Adams PD, Gros P. Modelling dynamics in protein crystal structures by ensemble refinement. *Elife.* 2012;1:e00311.
66. Liebschner D, Afonine PV, Baker ML, et al. Macromolecular structure determination using X-rays, neutrons and electrons: recent developments in Phenix. *Acta Crystallogr D Struct Biol.* 2019;75(Pt 10):861-877.
67. Emsley P, Cowtan K. Coot: model-building tools for molecular graphics. *Acta Crystallogr D Biol Crystallogr.* 2004;60(Pt 12 Pt 1):2126-2132.
68. Punjani A, Rubinstein JL, Fleet DJ, Brubaker MA. cryoSPARC: algorithms for rapid unsupervised cryo-EM structure determination. *Nat Methods.* 2017;14(3):290-296.